Enhanced Electric Double-Layer Capacitance by Desolvation of Lithium Ions in Confined Nanospaces of Microporous Carbon

Koki Urita,* Nozomi Ide, Kosuke Isobe, Hiroshi Furukawa, and Isamu Moriguchi

Graduate School of Engineering, Nagasaki University, 1-14 Bunkyo-machi, Nagasaki, Nagasaki 852-8521, Japan

ABSTRACT Carbon electrodes with specific microporous structures are strongly desired to improve the performance of electric double-layer capacitors (EDLCs). We report solvated states of Li ions in confined carbon micropores affecting specific capacitance. The average Li^+ solvation number of 1 M $LiClO_4$/propylene carbonate (PC) electrolyte introduced into porous carbon electrodes was determined using Raman spectroscopy and ^7Li NMR. Micropores with slightly larger pore size against the solvated molecules and the narrow two-dimensional spaces decreased the solvation number, enhancing specific capacitance. Hence, specific carbon morphology may be related to high EDL capacitance, and micropore structure is important in obtaining highly capacitive EDLC materials.

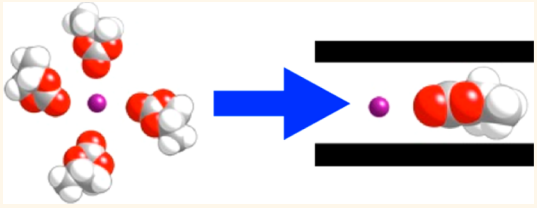

KEYWORDS: EDLC · ^7Li NMR · desolvation · microporous carbon

Porous carbon materials with high specific surface areas (SSAs) have been widely used as electrode materials for electric double-layer capacitors (EDLCs), which are functionalized by formation of an electric double layer (EDL) at the electrolyte/electrode interface.[1,2] The high SSA relative to pore size is actually provided by microporous carbon with a pore size of <2 nm. The micropores in high-SSA carbon have generally been believed to be too small to be accessible to solvated ions in an electrolyte and, thus, not to contribute to EDL capacitance of porous carbon. Instead, mesoporous materials have been considered to have the ideal structure for EDLC electrodes.[3,4] However, recent research on the effect of micropores on EDLC capacitance has focused on microporous carbon as applied to EDLC electrodes. Ohkubo *et al.* first reported a partial dehydration of ions in slit-shaped carbon micropores different from that in the bulk aqueous solution,[5] and this prompted the research on microporous EDLC materials to consider the effect of solvation state of electrolyte ions on their properties. Gogotsi *et al.* and Simon *et al.* reported that specific EDL capacitance based on surface area greatly increased on carbide-derived carbon materials in an acetonitrile electrolyte solution of $NEt_4 \cdot BF_4$ or a 1-ethyl-3-methylimidazolium-bis(trifluoromethylsulfnyl)imide (EMI-TFSI) ionic liquid when the average micropore size of the carbon was similar to the size of the electrolyte ions used.[6−8] The enhanced capacitance in a microporous carbon structure was also theoretically reported.[9] The enhancement in EDL capacitance was ascribed to desolvated electrolyte ions derived from spatial restriction by the micropores. The desolvated electrolyte ions can approach the electrode surface more closely, decreasing the thickness of the EDL (d). Consequently, the specific capacitance (C/A) is increased according to $C/A = e_r e_0/d$, where C is the specific capacitance per weight, A is the specific surface area of the electrode, and e_r and e_0 are the dielectric constants of the electrolyte and vacuum, respectively. Although the orientations of the electrolytes in the micropores were also reported,[10−12] morphological questions concerning the micropores remain unsolved; it

* Address correspondence to urita@nagasaki-u.ac.jp.

Received for review January 10, 2014 and accepted March 19, 2014.

Published online March 19, 2014
10.1021/nn500169k

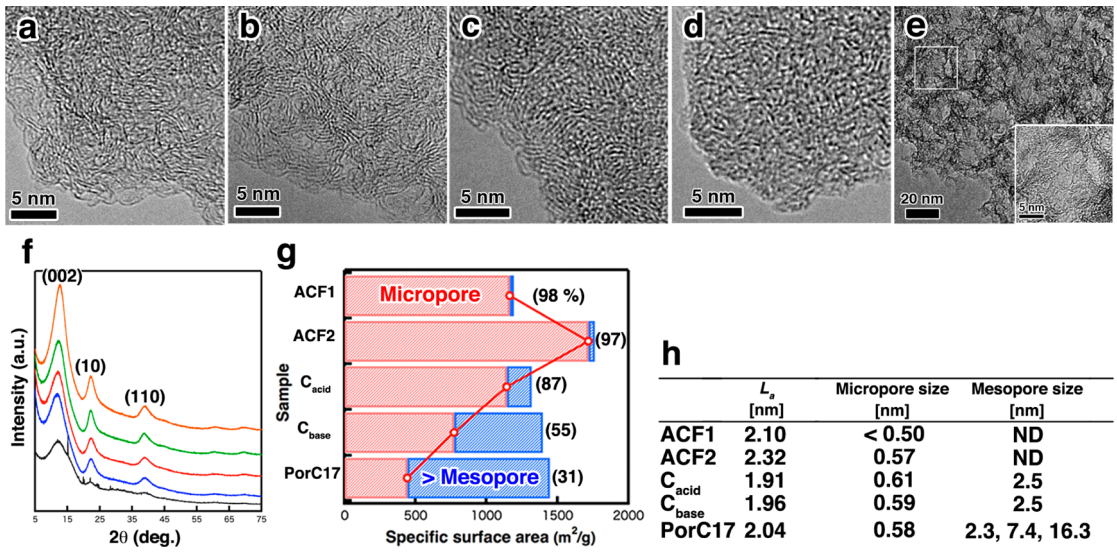

	L_a [nm]	Micropore size [nm]	Mesopore size [nm]
ACF1	2.10	< 0.50	ND
ACF2	2.32	0.57	ND
C_{acid}	1.91	0.61	2.5
C_{base}	1.96	0.59	2.5
PorC17	2.04	0.58	2.3, 7.4, 16.3

Figure 1. HR-TEM images showing carbon frameworks for (a) ACF1, (b) ACF2, (c) C_{acid}, (d) C_{base}, and (e) PorC17. The inset shows an enlarged image of the white square area in (e). (f) Synchrotron XRD patterns of ACF1 (orange), ACF2 (green), C_{acid} (red), C_{base} (blue), and PorC17 (black). The indexed peaks are diffraction planes of micrographite constituting the carbon framework. (g) SSAs for the samples. Numbers in parentheses indicate the percent micropore surface area of the total SSA. (h) Width of the graphitic crystallite (L_a) calculated from the (10) planes of the XRD profiles and average micropore and mesopore sizes. Micropore sizes of >0.50 nm were determined by the HK method. The mesopore size was determined by the DH method for PorC17 and by the INNES method otherwise.

is not clear why all microporous carbons do not show such high specific EDL capacitance and which structures are important for improving EDLC performance. The hypothesis relating to desolvation of electrolyte ions in micropores and its relation to EDL capacitance requires further experimental investigation to obtain high-performance EDLCs. We investigated the solvated state of Li ions in various porous carbon materials and the relationship between the EDL capacitance of porous carbon and the solvated state of the ions as well as pore structure (pore size and shape). Although previous reports discussed the desolvation state of NEt_4BF_4 electrolyte from the chemical shift caused indirectly by the aromatic carbon electrode surface (magnetic shielding with ring current),[13,14] the present study adopted the $LiClO_4$/PC (PC = propylene carbonate) electrolyte and liquid ^{7}Li NMR technique, where the chemical shifts are directly affected by the PC-solvation state of Li^+ because of strong interaction with the carbonyl (C═O) group of the PC molecule with a diamagnetic shielding effect. The present report should contribute significantly toward developing not only EDLCs but also Li ion secondary batteries (LIBs), because desolvation of Li^+ at the electrode interface is one of the key reactions of LIB electrodes and decreasing its activation energy will enhance LIB performance.[15]

RESULTS AND DISCUSSION

We characterized commercial activated carbon fibers (ACF1 and ACF2), newly developed organic–inorganic hybrid polymer-derived porous carbon materials (C_{acid} and C_{base}),[16] and a silica opal-derived porous carbon (PorC17) synthesized by the reported procedure.[17] C_{acid} and C_{base} were synthesized by a new method consisting of sol–gel reactions of a hybrid polymer with covalently bonded phenolic oligomer and siloxane parts. This synthetic method has the advantage of yielding microporous carbon materials with a relatively narrow pore size distribution controlled by acidic and basic catalysts.

The morphologies and porosities of the porous carbon samples were examined by transmission electron microscope (TEM), N_2 adsorption isotherm, and synchrotron X-ray diffraction (XRD) measurements. The TEM images clearly revealed carbon frameworks consisting of micrographite of various sizes (Figure 1a–d and inset of e). The ACFs, C_{acid}, and C_{base} had massive structures. PorC17 had mesopores originating from the template SiO_2 particles ~17 nm in diameter (Figure 1e, inset). We have calculated the in-plane crystallite size of the micrographites constituting the pore walls of our samples from the (10) reflection in the XRD profiles (Figure 1f,h). Certain sharp XRD peaks for PorC17 were attributed to a sample holder obstructing the X-ray path. The ACFs had wider plane sizes of micrographites than the other materials, indicating that the ACFs had a developed graphitic structure in the *ab*-plane. C_{acid} and C_{base} formed sponge-like structures, as illustrated in the TEM images. The presence of mesopores in C_{acid}, C_{base}, and PorC17 was also confirmed by the N_2 adsorption isotherms (Supporting Figure S1a). The SSAs were carefully estimated by applying the α_s-method,[18,19] an optimized method for determining the porosities of microporous carbon materials, to the N_2 adsorption isotherms (Figure 1g). The results

allowed us to classify the samples based on the percent micropore surface area: the ACFs and C_{acid} were regarded as microporous, while C_{base} and PorC17 were regarded as a micro/mesoporous and mesoporous, respectively. The difference in the porous structures between C_{acid} and C_{base} likely resulted from the polymerization mechanism of the siloxane part depending on the catalyst. It has been reported that slow 1-D and rapid 3-D polymerization of silicate occurs preferentially under acidic and basic conditions, respectively.[20] Rapid 3-D polymerization during the sol−gel reaction in the hybrid polymer solution results in formation of massive silica that would become mesopores in C_{base} after hydrofluoric acid (HF) etching.

The pore size distributions (PSDs) of the samples were further analyzed by the Horvath−Kawazoe (HK) method for the micropores (Supporting Figure S1b)[21] and the Dollimore and Heal (DH) or Innes method for the mesopores (Supporting Figure S1c).[22,23] The average pore sizes of the micropores and mesopores determined from the PSDs are shown in Figure 1H. The mesopore size range was 2.3−2.5 nm for C_{acid}, 2.2−6.0 nm for C_{base}, and 2.1−2.7, 7.0−20 nm for PorC17. All samples had micropores of <0.82 nm, which corresponds to the Stokes' diameter of Li^+ in propylene carbonate used as an electrolyte in this study. Most of the micropores in the ACFs were <0.57 nm, similar to the short axis length of the PC molecule (0.54 nm).

The electrochemical properties of the samples were evaluated by galvanostatic charge/discharge measurements in a 1 M $LiClO_4$/PC electrolyte solution at room temperature. The third discharge curves for the samples are shown in Figure 2a because charging/discharging became stable after the third cycle. Other than ACF1, the samples showed typical discharge curves for EDLs. The EDL capacitances were dominated by Li^+, which contributes to the formation of the EDL at the negatively charged electrode surface below the open circuit voltage (OCV). Li^+ was expected to be a good probe for investigating the effects of micropores on EDL capacitance and the solvated state of electrolyte ions because the Stokes' diameter of Li^+ in PC is similar to the micropore size of the samples. Figure 2b shows the specific capacitance normalized to the SSA, estimated from the slope of the curve in the potential range below the OCV. The hybrid polymer-derived samples (C_{acid} and C_{base}) had higher specific capacitance than did PorC17, indicating that their micropore surfaces strongly affected EDLC performance. Because most of the micropores in C_{acid} and C_{base} were smaller than the Stokes' diameter of Li^+ in PC (0.82 nm), desolvated Li ions are assumed to have contributed to formation of the EDL in the micropores. On the other hand, the specific capacitance of the microporous ACF samples was

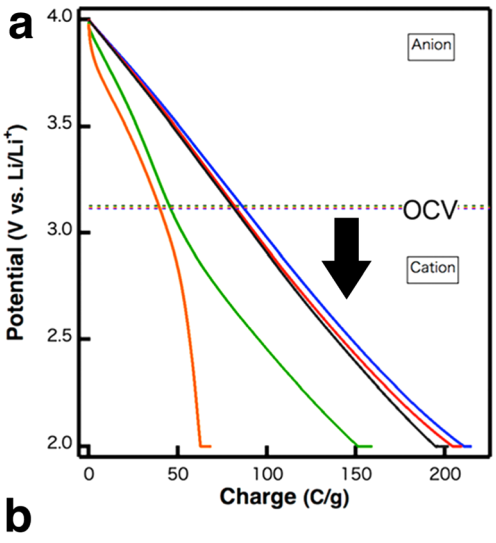

Sample	Specific capacitance [μF/cm^2]
ACF1	2.2
ACF2	6.1
C_{acid}	9.6
C_{base}	8.7
PorC17	7.2

Figure 2. (a) Third discharge curves obtained in the CC−CV mode at a current density of 10 mA/g for ACF1 (orange), ACF2 (green), C_{acid} (red), C_{base} (blue), and PorC17 (black). (b) Specific capacitance normalized by the SSA determined from the slope of the discharge curve in the potential range below the OCV.

lower than those of C_{acid}, C_{base}, and PorC17; ACF1 had a particularly low EDL capacitance. The ACF samples had many micropores smaller than or similar to the short-axis length of the PC molecule (0.54 nm; Supporting Figure S1d). Thus, the electrolyte had limited access to the micropore surfaces. Therefore, the specific capacitance normalized to the SSA would be expected to be lower for the ACF samples than for the other materials.

^{7}Li NMR measurements were carried out to clarify the solvation state of Li^+ in the porous carbon materials and its relationship to EDL capacitance. The porous carbon samples vacuum-impregnated with a 1 M $LiClO_4$/PC solution showed NMR peaks that were deconvoluted into 1−3 peaks (Figure 3a). We also examined ^{7}Li NMR spectra for $LiClO_4$/PC electrolyte solutions with varying concentrations from 0.8 to 2.0 M to elucidate the relationship between the chemical shift and average solvation number of Li^+. The NMR peaks shifted toward higher magnetic fields with increasing concentration (Supporting Figure S2c). The results are in agreement with the data reported by Y. M. Cahen *et al.*[24] The formation of a contact ion pair strongly depends on both the donor number and the bulk

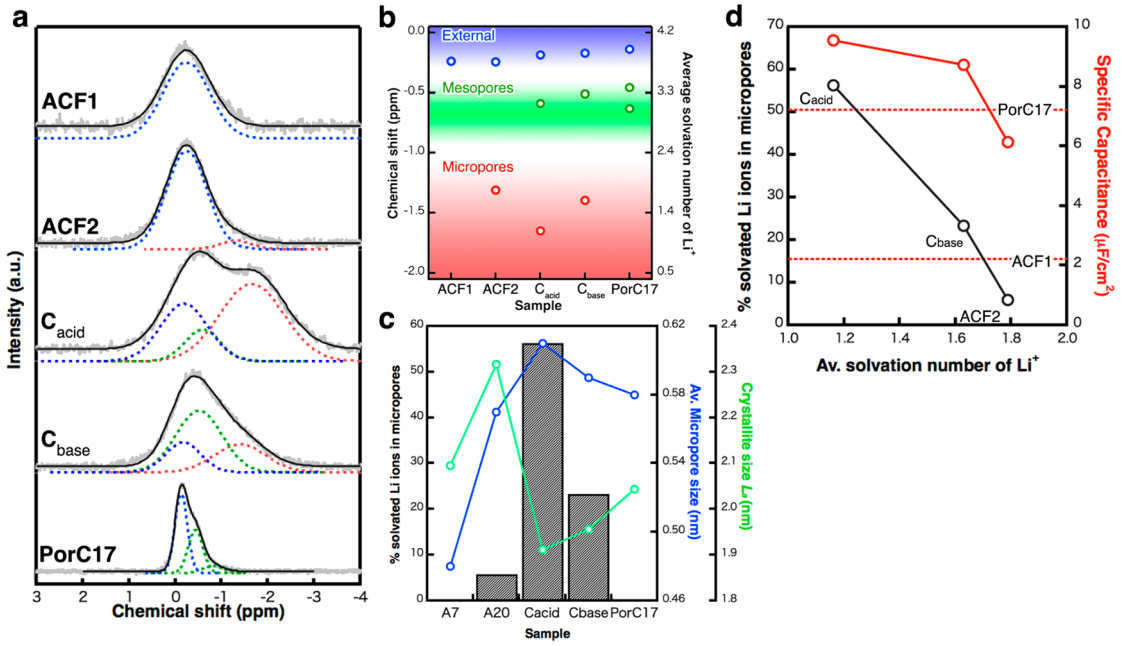

Figure 3. (a) ^{7}Li NMR spectra (gray) of porous carbon samples with deconvoluted peaks corresponding to solvated Li^+ on external surfaces or in macropores (blue), in mesopores (green), and in micropores (red) of the samples and the fitted curves (black). (b) Chemical shifts and the average solvation numbers of PC molecules for Li^+ classified by pore size range. (c) Percent presence of solvated Li^+ in micropores (bar chart), average micropore size (blue), and the crystallite size (L_a) of micrographites constructing pore walls (green) of the samples. (d) Relationship between the percent presence of solvated Li^+ in the micropores, the specific capacitance, and the average solvation number of the PC molecules for Li^+ in the micropores for ACF2, C_{acid}, and C_{base}. The red broken lines show the specific capacitances of ACF1 and PorC17.

dielectric constant of the solvent molecule, which for PC are 15.1 and 65, respectively. Therefore, the chemical shifts are strongly affected by the diamagnetic shielding effect of the C═O group of the PC molecule, and the upfield shift is mainly due to a weakened interaction between Li^+ ions and PC molecules. Here the interaction was evaluated by Raman spectroscopy as an average solvation number of PC molecules per Li ion.[25] Figure 3b illustrates the average solvation number of the porous carbon samples determined by applying the relationship between the chemical shift and the average solvation number in Supporting Figure S2. Also, taking into account the porosities of the samples and a previous theoretical study,[26] the average solvation numbers corresponding to each deconvoluted NMR peak in Figure 3a were assigned to Li ions in micropores, in mesopores, and on the external surface (including macropores). The peak around 0 ppm of each spectrum (blue peaks in Figure 3a) was assigned to Li ions on the external surface or in macropores, since the chemical shift is given in ppm relative to a 1 M $LiClO_4$/PC solution. It is also explained by the average solvation number of the PC molecules on the external surface or in the macropores being 3.6−4.4, similar to the reported value for the bulk solution.[25−27] The average solvation number decreased for the Li ions confined to carbon nanopores, particularly micropores. The decrease in micropores agrees reasonably well with the previous theoretical study.[26] They indicated that when a Li^+-4PC complex adsorbs in a micropore with a pore size of 0.6 nm, desolvation occurs and the number of solvated PC molecules is decreased below 2, but at least one PC molecule can remain as the Li^+-PC complex. Accordingly, the NMR peaks for the ACF samples, which are microporous carbon materials without mesopores, suggested that Li ions are present in the micropores (red peaks in Figure 3a) and/or on the external surface (blue peaks in Figure 3a). Because the micropore size of ACF1 is too small to allow access by the PC molecule and solvated Li^+, ACF1 exhibited only the peak assignable to Li ions on the external surface. The spectra for the C_{acid} and C_{base} samples with micro- and mesopores showed three Li ion states: in the micropores, in the mesopores (green peaks in Figure 3a), and on the external surface. Since the green ones in Figure 3a are not present in microporous ACF samples and the average solvation number was larger than that in micropores theoretically determined,[26] they should be derived from Li ions in mesopores. That for PorC17 showed two Li ion states, in the mesopores and on the external surface because the pore structure of PorC17 is mainly formed by mesopores with the pore size range 2.1−2.7 and 7.0−20 nm (Supporting Figure S1c). PorC17 does have some micropores, but an NMR peak for Li ions in the micropores should not be detected because of the relatively small number of micropores (Figure 1g). Figure 3c summarizes the average pore size of the micropores and the in-plane crystallite size of the micrographite, as well as the percentage of Li ions in

the micropores estimated from the deconvoluted NMR peak areas. The Li ions were hindered from entering the micropores of the ACF samples. ACF2 had a smaller percentage of Li ions in the micropores and a slightly larger average solvation number for the Li ions compared to C_{acid} and C_{base}, although their micropore size distribution of ~0.54−1.0 nm was nearly the same. Strong interactions with the wide carbon wall of the micropores in ACF2 likely restricted the access of PC-solvating Li ions to the micropores.[28] The micropores of C_{acid} and C_{base}, constructed with short lateral size, were more accessible to the PC-solvating Li ions, promoting desolvation of the PC molecules in micropores with a size similar to the Stokes' diameter of Li^+ in PC. Figure 3d illustrates the relationship between the specific capacitance and the solvation number, as well as the percentage of Li ions located in the micropores. Compared with mesoporous PorC17, microporous C_{acid} and micro/mesoporous C_{base} had higher specific capacitance, but microporous ACF samples had lower specific capacitance. This behavior is closely related to the percentage of Li ions in the micropores; although the Li ion was located only on the external surface of ACF1 and was hindered from entering the micropores in ACF2 by the narrow pore size, C_{acid} and C_{base} form suitable pore structures (micropore size and shape) for solvating Li^+ to be desolvated in the micropores.

CONCLUSION

We experimentally identified which microporous structures were most effective in desolvating Li^+ to enhance EDL capacitance. Our NMR analysis revealed a marked decrease in the solvation number of Li^+ in the micropores resulting from spatial confinement. Because desolvation decreases the distance between the electrode surface and electrolyte ions, the specific capacitance improves with a decrease in the average solvation number as well as an increase in the percentage of Li ions located in the micropores. These results clearly indicate the key role of a specific structure with a micropore size around the Stokes' diameter of Li^+ in PC in producing a smaller solvation number and higher percentage of Li^+ in the micropores, resulting in higher EDL capacitance normalized to surface area. We consider that this particular micropore structure with confined but relatively weak interaction for rearrangement of solvated ions is quite important for enhancing the specific capacitance. These results explain why all microporous carbon materials do not show high specific EDL capacitance, and the morphological information on microporous carbon materials may facilitate the design of optimal electrodes with high EDL capacitance.

MATERIALS AND METHODS

Synthesis of Porous Carbon Materials. We used commercial activated carbon fibers (ACF1 and ACF2) with different pore sizes kindly supplied by Ad'All Co., Ltd. The other porous carbon materials were synthesized as described below. Micro- and micro/mesoporous carbon materials were synthesized from an organic−inorganic hybrid polymer consisting of a phenolic part and siloxane part (COMPOCERAN (P502), kindly supplied by Arakawa Chemical Industries Ltd.; see ref 16 for the chemical structure). An ethanol solution of P502 was converted into a gel by adding aqueous HCl or aqueous NH_3 as a catalyst under stirring, and then the gel was heated at 443 K for 30 min in air and at 1273 K for 5 h under Ar gas. The obtained SiO_2/carbon nanocomposites were subjected to HF etching and dried to yield porous carbon materials. The porous carbon materials synthesized using the HCl and NH_3 catalysts were denoted C_{acid} and C_{base}, respectively. A mesoporous carbon material was synthesized by a SiO_2-opal template method as previously reported.[17] A SiO_2-opal crystal was obtained by centrifugation of a SiO_2 colloidal solution with an average particle diameter of 17 nm (Cataloid SI-40, JGC Catalysts and Chemicals Ltd.) and dried *in vacuo* for 1 day. The opal crystal was immersed in a mixed solution of phenol and formaldehyde with a few drops of 35 wt % aqueous HCl. After separation from the solution, the opal was heated at 400 K for 12 h in air and at 1273 K under Ar gas to yield a SiO_2-opal/carbon nanocomposite. The mesoporous carbon material, referred to as PorC17, was obtained by HF etching of the SiO_2-opal/carbon nanocomposite and drying. The amount of residual SiO_2 was confirmed by thermogravimetric analysis to be less than 1 wt %.

Microstructural Characterization. Morphological information for the samples was directly obtained using a TEM (JEOL JEM-2010 UHR) operated at 120 kV with a rapid imaging CCD camera (Gatan ORIUS SC1000). Prior to TEM observation, the specimens were ultrasonically dispersed in ethanol, depositing the droplets onto a Cu grid covered with a carbon membrane. The SSA and pore size analysis were performed using a Belsorp-Max instrument (BEL Japan, Inc.), which can measure an adsorption isotherm with relative pressure on the order of 10^{-8}, corresponding to a pore size of ~0.35 nm. All adsorption isotherms were measured after pretreatment of the samples under vacuum at 423 K for 2 h. Powder XRD patterns were collected using synchrotron radiation X-rays (λ = 0.7887 nm) in the BL02B2 beamline of SPring-8, Japan. The samples were sealed in 0.5 mm Lindemann glass capillaries (Hilgenberg GmbH) for analysis.

Electrochemical Analysis. Electrochemical charge/discharge curves were measured with an electrochemical analyzer (HJ-SD-8, Hokuto Denko) at room temperature in a sealed three-electrode cell equipped with metallic Li foil on Ti mesh as counter and reference electrodes. The electrolyte was a 1 M solution of $LiClO_4$ in PC. The porous carbon samples were mixed with polytetrafluoroethylene at a weight ratio of 92:8 and then were pressed onto the Ti mesh as a working electrode. Charging/discharging was carried out in constant current−constant voltage (CC−CV) mode; the current density of the CC mode was set at 10 mA/g, and the potential range was 2−4 V *vs* Li/Li^+.

Solvated State Analysis. The solvated state of Li^+ in the $LiClO_4$/PC solution was estimated by Raman spectroscopy (JASCO NRS-3000, 532 nm laser) and ^7Li NMR spectroscopy (JEOL JNM-AL400NMR, 400 MHz where 1 M $LiClO_4$ aqueous and CD_3OH were used as the external standard at 298 K). Electrolyte solutions (0.8−2.0 M) of $LiClO_4$/PC were prepared in a glovebox under Ar atmosphere, and sealed glass tubes filled with the solutions were used for the measurements. The average solvation number of the PC molecules per Li^+ dependent on the concentration of the $LiClO_4$/PC solution was determined from

the Raman spectra based on previous reports (see Supporting refs 1−4). We then obtained the relationship between the solvation number and the ^{7}Li NMR chemical shift of the $LiClO_4$/PC solution. The solvated state of Li^+ in the porous carbon materials was evaluated using the relationships obtained from the ^{7}Li NMR peaks for the $LiClO_4$/PC solution-impregnated porous carbon materials. NMR chemical shifts are given in ppm relative to a 1 M $LiClO_4$/PC solution. The electrolyte-impregnated porous carbon materials were prepared as follows: (1) pretreatment of the porous carbon materials at 423 K for 2 h *in vacuo*, (2) impregnation of 1 M $LiClO_4$/PC solution into the porous carbon materials, and (3) removal of the residual electrolytes after holding the impregnated samples in the NMR tubes overnight.

Conflict of Interest: The authors declare no competing financial interest.

Acknowledgment. This study made use of instruments (TEM and NMR) at the Center for Instruments Analysis of Nagasaki University. The authors would like to thank Y. Ohama for assistance with the ^{7}Li NMR measurements and T. Fujimori for many helpful discussions. The synchrotron radiation experiments were performed at the BL02B2 of SPring-8 with the approval of the Japan Synchrotron Radiation Research Institute (JASRI) (Proposal No. 2011B1559). This work was partially supported by a Grant-in-Aid for Scientific Research from the Ministry of Education, Culture, Sports, Science, and Technology of Japan (Young Scientists (B) No. 24710122 and Scientific Research (B) No. 5288110).

Supporting Information Available: Porosity characterization of porous carbons and model of the electrolyte solvent molecule; N_2 adsorption isotherm, the pore size distribution curve, and structural model of the propylene carbonate molecule. Determination method for the relationship between chemical shifts in ^{7}Li NMR spectra and the average solvation number of Li^+. Relationship between the average solvation number and the chemical shift; Raman spectra, a vibration model of symmetric ring deformation, ^{7}Li NMR, and average solvation number for each chemical shift. This material is available free of charge *via* the Internet at http://pubs.acs.org.

REFERENCES AND NOTES

1. Frackowiak, E.; Béguin, F. Carbon Materials for the Electrochemical Storage of Energy in Capacitors. *Carbon* **2001**, *39*, 937–950.
2. Simon, P.; Gogotsi, Y. Materials for Electrochemical Capacitors. *Nat. Mater.* **2008**, *7*, 845–854.
3. Lee, J.; Yoon, S.; Hyeon, T.; Oh, S. M.; Kim, B. K. Synthesis of a New Mesoporous Carbon and its Application to Electrochemical Double-Layer Capacitors. *Chem. Commun.* **1999**, 2177–2178.
4. Zhou, H.; Zhu, S.; Hibino, M.; Honma, I. Electrochemical Capacitance of Self-Ordered Mesoporous Carbon. *J. Power Sources* **2003**, *122*, 219–223.
5. Ohkubo, T.; Konishi, T.; Hattori, Y.; Kanoh, H.; Fujikawa, T.; Kaneko, K. Restricted Hydration Structures of Rb and Br Ions Confined in Slit-Shaped Carbon Nanospace. *J. Am. Chem. Soc.* **2002**, *124*, 11860–11861.
6. Chmiola, J.; Yushin, G.; Gogotsi, Y.; Portet, C.; Simon, P.; Taberna, P.-L. Anomalous Increase in Carbon Capacitance at Pore Sizes Less Than 1 Nanometer. *Science* **2006**, *313*, 1760–1763.
7. Largeot, C.; Portet, C.; Chmiola, J.; Taberna, P.-L.; Gogotsi, Y.; Simon, P. Relation between the Ion Size and Pore Size for an Electric Double-Layer Capacitor. *J. Am. Chem. Soc.* **2008**, *130*, 2730–2731.
8. Lin, R.; Taberna, P.-L.; Chmiola, J.; Guay, D.; Gogotsi, Y.; Simon, P. Microelectrode Study of Pore Size, Ion Size, and Solvent Effects on the Charge/Discharge Behavior of Microporous Carbons for Electrical Double-Layer Capacitors. *J. Electrochem. Soc.* **2009**, *156*, A7–A12.
9. Merlet, C.; Rotenberg, B.; Madden, P. A.; Taberna, P.-L.; Simon, P.; Gogotsi, Y.; Salanne, M. On the Molecular Origin of Supercapacitance in Nanoporous Carbon Electrodes. *Nat. Mater.* **2012**, *11*, 306–310.
10. Jiang, D.-E.; Jin, Z.; Henderson, D.; Wu, J. Solvent Effect on the Pore-Size Dependence of an Organic Electrolyte Supercapacitor. *J. Phys. Chem. Lett.* **2012**, *3*, 1727–1731.
11. Tanaka, A.; Iiyama, T.; Ohba, T.; Ozeki, S.; Urita, K.; Fujimori, T.; Kanoh, H.; Kaneko, K. Effect of a Quaternary Ammonium Salt on Propylene Carbonate Structure in Slit-Shape Carbon Nanopores. *J. Am. Chem. Soc.* **2010**, *132*, 2112–2113.
12. Fukano, M.; Fujimori, T.; Ségalini, J.; Iwama, E.; Taberna, P.-L.; Iiyama, T.; Ohba, T.; Kanoh, H.; Gogotsi, Y.; Simon, P. Vertically Oriented Propylene Carbonate Molecules and Tetraethyl Ammonium Ions in Carbon Slit Pores. *J. Phys. Chem. C* **2013**, *117*, 5752–5757.
13. Wang, H.; Köster, T. K. J.; Trease, N. M.; Ségalini, J.; Taberna, P.-L.; Simon, P.; Gogotsi, Y.; Grey, C. P. Real-Time NMR Studies of Electrochemical Double-Layer Capacitors. *J. Am. Chem. Soc.* **2011**, *133*, 19270–19273.
14. Forse, A. C.; Griffin, J. M.; Wang, H.; Trease, N. M.; Presser, V.; Gogotsi, Y.; Simon, P.; Grey, C. P. Nuclear Magnetic Resonance Study of Ion Adsorption on Microporous Carbide-Derived Carbon. *Phys. Chem. Chem. Phys.* **2013**, *15*, 7722–7730.
15. Abe, T.; Fukuda, H.; Iriyama, Y.; Ogumi, Z. Solvated Li-Ion Transfer at Interface between Graphite and Electrolyte. *J. Electrochem. Soc.* **2004**, *151*, A1120–A1123.
16. Aono, S.; Tsurudo, T.; Urita, K.; Moriguchi, I. Direct Synthesis of Novel Homogeneous Nanocomposites of Li_2MnSiO_4 and Carbon as a Potential Li-Ion Battery Cathode Material. *Chem. Commun.* **2013**, *49*, 2939–2941.
17. Moriguchi, I.; Nakahara, F.; Furukawa, H.; Yamada, H.; Kudo, T. Colloidal Crystal-Templated Porous Carbon as a High Performance Electrical Double-Layer Capacitor Material. *Electrochem. Solid-State Lett.* **2004**, *7*, A221–A223.
18. Sing, K. S. W. The Use of Physisorption for the Characterization of Microporous Carbons. *Carbon* **1989**, *27*, 5–11.
19. Kaneko, K.; Ishii, C. Superhigh Surface Area Determination of Microporous Solids. *Colloids Surf., A* **1992**, *67*, 203–212.
20. Livage, J.; Henry, M.; Sanchez, C. Sol-Gel Chemistry of Transition Metal Oxides. *Prog. Solid State Chem.* **1988**, *18*, 259–341.
21. Horváth, G.; Kawazoe, K. Method for the Calculation of Effective Pore Size Distribution in Molecular Sieve Carbon. *J. Chem. Eng. Jpn.* **1983**, *16*, 470–475.
22. Dollimore, D.; Heal, G. R. An Improved Method for the Calculation of Pore Size Distribution from Adsorption Data. *J. Appl. Chem.* **2007**, *14*, 109–114.
23. Innes, W. B. Use of Parallel Plate Model in Calculation of Pore Size Distribution. *Anal. Chem.* **1957**, *29*, 1069–1073.
24. Cahen, Y. M.; Handy, P. R.; Roach, E. T.; Popov, A. I. Spectroscopic Studies of Ionic Solvation. XVI. Lithium-7 and Chlorine-35 Nuclear Magnetic Resonance Studies in Various Solvents. *J. Phys. Chem.* **1975**, *79*, 80–85.
25. Yamada, Y.; Koyama, Y.; Abe, T.; Ogumi, Z. Correlation between Charge−Discharge Behavior of Graphite and Solvation Structure of the Lithium Ion in Propylene Carbonate-Containing Electrolytes. *J. Phys. Chem. C* **2009**, *113*, 8948–8953.
26. Ohtani, H.; Hirao, Y.; Ito, A.; Tanaka, K.; Hatozaki, O. Theoretical Study on Thermochemistry of Solvated Lithium-Cation with Propylene Carbonate. *J. Therm. Anal. Calorim.* **2010**, *99*, 139–144.
27. Ohtaki, H. Structural Studies on Solvation and Complexation of Metal Ions in Nonaqueous Solutions. *Pure Appl. Chem.* **1987**, *59*, 1143–1150.
28. Ohba, T.; Kaneko, K.; Kanoh, H. Local Ordered Structure of Propylene Carbonate in Slit-Shaped Carbon Nanopores by GCMC Simulation. *ISRN Nanotechnol.* **2011**, *2011*, 5.